Characterizing friction in sliding isolation bearings

Manish Kumar[1,*,†], Andrew S. Whittaker[1] and Michael C. Constantinou[1]

[1]*Department of Civil, Structural and Environmental Engineering, University at Buffalo, Buffalo, NY, 14260*

SUMMARY

The force-displacement behavior of the Friction Pendulum™ (FP) bearing is a function of the coefficient of sliding friction, axial load on the bearing and effective radius of the sliding surface. The coefficient of friction varies during the course of an earthquake with sliding velocity, axial pressure and temperature at the sliding surface. The velocity and axial pressure on the bearing depend on the response of the superstructure to the earthquake shaking. The temperature at an instant in time during earthquake shaking is a function of the histories of the coefficient of friction, sliding velocity and axial pressure, and the travel path of the slider on the sliding surface. A unified framework accommodating the complex interdependence of the coefficient of friction, sliding velocity, axial pressure and temperature is presented for implementation in nonlinear response-history analysis. Expressions to define the relationship between the coefficient of friction and sliding velocity, axial pressure, and temperature are proposed, based on available experimental data. Response-history analyses are performed on FP bearings with a range of geometrical and liner mechanical properties, and static axial pressure. Friction is described using five different models that consider the dependence of the coefficient of friction on axial pressure, sliding velocity and temperature. Frictional heating is the most important factor that influences the maximum displacement of the isolation system and floor spectral demands if the static axial pressure is high. Isolation system displacements are not significantly affected by considerations of the influence of axial pressure and velocity on the coefficient of friction.

1. INTRODUCTION

Friction Pendulum™ (FP) bearings are used in the United States to seismically isolate structures. In its single concave configuration, the FP bearing comprises a sliding surface of polished stainless steel and an articulated slider coated with PTFE-type composite material. Figure 1 is a section through a single concave FP bearing.

For constant values of axial load and coefficient of sliding friction, the force-displacement behavior of an FP bearing in a horizontal direction can be represented by the bilinear relationship of Figure 2. The relationship is characterized by a characteristic strength Q

* Correspondence to: Manish Kumar, Department of Civil, Structural and Environmental Engineering, University at Buffalo, Buffalo, NY, 14260
† E-mail: mkumar3@buffalo.edu

This is the author manuscript accepted for publication and has undergone full peer review but has not been through the copyediting, typesetting, pagination and proofreading process, which may lead to differences between this version and the Version of Record. Please cite this article as doi: 10.1002/EQE.2524

(the product of the coefficient of friction and the axial load) and a post-yield stiffness K (the ratio of the supported axial load to the radius of curvature of the bearing). In practice, the axial load on a bearing in an isolation system changes continuously during an earthquake because the superstructure responds to the vertical and horizontal shaking, which leads to continuous changes in Q and K.

The evolution of the mechanical properties of sliding isolators during an earthquake are accommodated in design of buildings and bridges using bounding values on Q and K, via property modification factors [1,2,3]. These factors are intended to account for the effects of ageing and travel that might accrue after isolator installation and before the design event. Analysis using the bounding values is intended to bracket the mean response of the isolation system to earthquake shaking. For nuclear structures, distributions of isolation-system response are used for design and risk assessment, and the bounding methods of analysis are insufficient. For such facilities, it is critical that each component be analyzable for design basis and beyond design basis shaking, which requires the mechanical models of isolators to evolve over the course of a response-history analysis. Developing the techniques and tools to do so for the coefficient of sliding friction is the focus of this paper.

The coefficient of sliding friction is a function of the instantaneous values of sliding velocity, axial pressure on the bearing and temperature at the sliding surface, which further changes Q. The temperature at the sliding surface at a given instant depends on the histories of sliding velocity, axial pressure and coefficient of friction, and the path traveled by the slider. The displacement, u_y, is set to 1 mm [4].

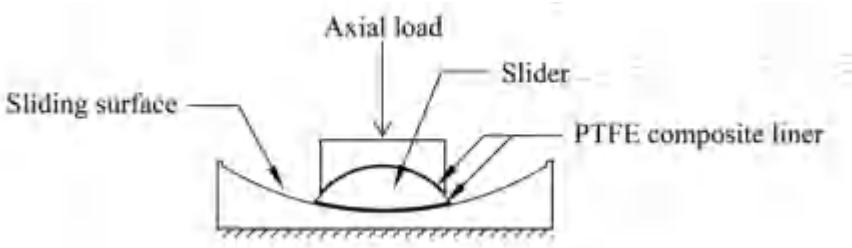

Figure 1. Section through a single concave Friction Pendulum™ (FP) bearing

The sliding velocity affects the coefficient of friction due to the viscous nature of the PTFE-type composite used for the liner. The coefficient increases with an increase in sliding velocity up to a constant value. The effect has been studied by Constantinou et al. [5] and the velocity dependence of friction has been incorporated in software such as SAP2000 [6] and OpenSees [7].

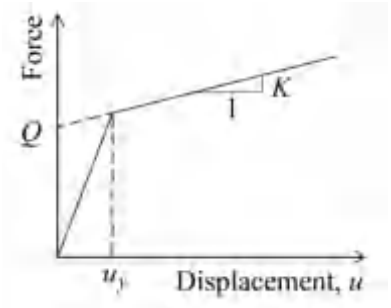

Figure 2. Lateral force-displacement relationship for an FP bearing

The characteristic strength is related to the shearing strength per unit area, *s*, of the liner, which increases with increasing axial pressure, p, up to a limiting value, $s_{\max}$: $s = a_o + a_1 p \le s_{\max}$, where a_o and a_1 are constants determined from experiments. The coefficient of friction, μ, the ratio of the shearing force to the axial force, is inversely proportional to pressure: $\mu = s / p = a_1 + a_o / p$ [3]. The variation in the coefficient of friction with axial pressure is a function of the velocity of sliding. Only the high-velocity coefficient of friction varies significantly with axial pressure; the small-velocity coefficient of friction is relatively unaffected [8]. Relationships between the coefficient of sliding friction and axial pressure have been incorporated in software such as 3D-BASIS-ME [9] and OpenSees.

A limited number of experiments have been performed (e.g., [3,10]) to characterize the relationship between the coefficient of friction and temperature at the contact surface. These experiments indicate that the coefficient decreases sharply with increasing temperature at lower temperatures, because of changes in the viscoelastic properties of the PTFE-type composite material. At higher temperatures, the rate of decrease is less and the coefficient trends to a constant value. The effect of temperature rise on the response of a structure isolated with sliding bearings will be greatest for those bearings composed of one sliding surface (the single concave FP bearing studied here) and less for bearings with multiple sliding surfaces (e.g., the Triple Friction Pendulum™ bearing [11]), for a given bearing pressure and liner material, because the heat flux is distributed to more than one sliding surface.

The primary objective of this study is to provide a unified treatment of the interdependence of the coefficient of friction, axial pressure, sliding velocity and temperature at the sliding surface for implementation in response-history analysis. The dependence of the coefficient of friction on sliding velocity, axial pressure and temperature is established first using available experimental data. Appropriate assumptions are made to decouple the influences of sliding velocity and axial pressure on the coefficient of friction. A method to compute temperature at the sliding surface over the course of a response-history analysis is presented. Five friction models are considered.

Response-history analyses are performed on macro-level single concave FP bearings with different geometrical properties and levels of axial load to characterize the effect of the choice of friction model on isolation-system displacements and floor spectral ordinates in the isolated

superstructure. In these analyses, the mass of the superstructure is assigned to the slider in the vertical and two horizontal directions, the slider is restrained from rotating about the two horizontal axes, and no additional damping is provided. The element *singleFPBearing* in the open-source program OpenSees [7] is used to model the bearing and its source code is modified to update the coefficient of friction at every step of analysis with sliding velocity, axial pressure and/or temperature on the sliding surface. Thirty sets of three-component ground motions are used for response-history analysis. Each component in each set is spectrally matched to either the vertical or horizontal Uniform Hazard Spectrum developed for the site of the Diablo Canyon Nuclear Generating Station in California for a return period of 10,000 years. These motions are expected to impose significant displacement demands on isolated structures, given the proximity of this site to major active faults. Information on the ground motions is provided in [4].

2. CHARACTERIZING THE COEFFICIENT OF FRICTION

Expressions to define the dependence of the coefficient of friction on sliding velocity, axial pressure and temperature at the sliding surface are presented in this section. A method to compute the temperature at the sliding surface during response-history analysis is described.

2.1 Dependence of the coefficient of friction on sliding velocity

The relationship between the coefficient of friction and sliding velocity is described by an exponential function of Mokha et al. [12]:

$$\mu(v) = \mu_{\max} \times \left(1 - \left(1 - \tilde{\mu}_v\right) e^{-av}\right) \tag{1}$$

where $\mu(v)$ is the coefficient of sliding friction, v is velocity, $\mu_{\max}$ is the coefficient of friction at very high sliding velocity, $\tilde{\mu}_v$ is the ratio of the coefficient of friction at very small velocity to $\mu_{\max}$, and a determines the shape of the relationship. The value of a is set to 100 s/m based on past studies [13]. A fixed value of $\tilde{\mu}_v$ allows $\mu(v)$ to be expressed as the product of $\mu_{\max}$ and a factor that depends only on sliding velocity. The parameter $\tilde{\mu}_v$ is set equal to 0.5, which is also consistent with past studies [14].

2.2 Dependence of the coefficient of friction on axial pressure

Figure 3 plots the coefficient of friction at high velocity versus axial pressure; the data are based on experiments involving liners of the type used in FP bearings manufactured in the United States [8,15,16,17]. Constantinou et al. [8] note that there is little effect of change in axial pressure on the coefficient of friction at small velocities for these liner materials. However, to simplify implementation, $\mu_{\min}$ is assumed to be $0.5\mu_{\max}$ for all levels of axial pressure, which may only affect response for weak ground motion that are of no practical interest.

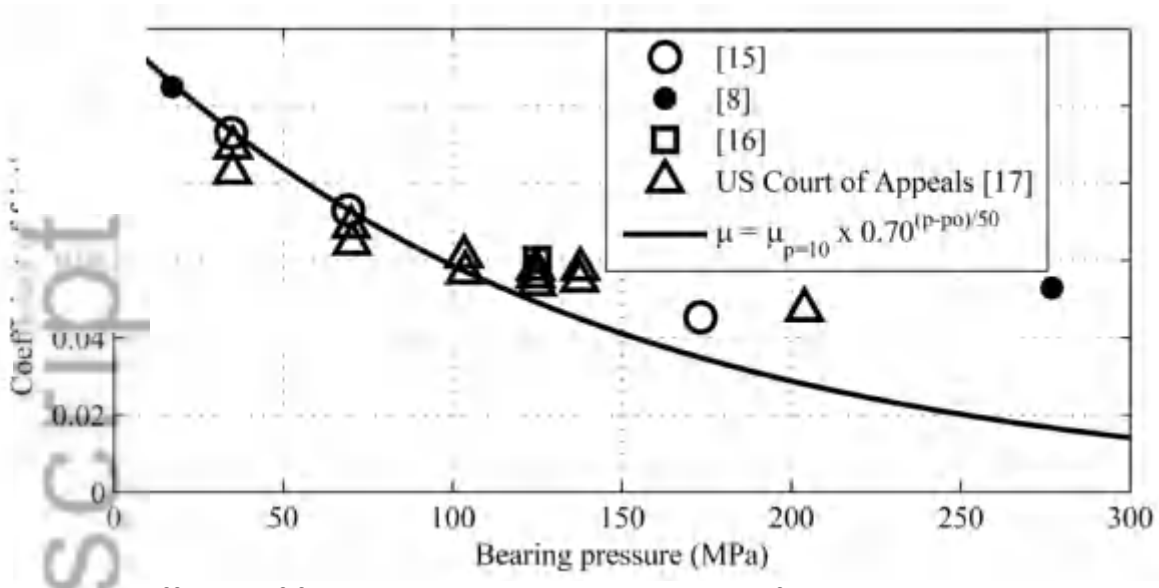

Figure 3. Coefficient of friction measured at a high velocity of sliding plotted against bearing pressure (adapted from Mokha et al. [17])

The experimentally recorded values of $\mu_{\max}$ in Figure 3 decrease with increasing axial pressure at pressures less than 100 MPa, and approach a constant value at even greater pressures. The asymptotic decay seen in the figure can be described using the following functional form:

$$\mu(p) = \mu_{p_o} \times \left(\tilde{\mu}_p + \left(1 - \tilde{\mu}_p\right) a_p^{h_p (p - p_o)} \right) \tag{2}$$

where $\mu(p)$ is the high-velocity coefficient of friction at axial pressure p, μ_{p_o} is the high-velocity coefficient of friction at the reference axial pressure p_o, $\tilde{\mu}_p$ is the ratio of the high-velocity coefficient of friction at a high axial pressure (e.g., 250 MPa) to μ_{p_o}, and a_p and h_p determine the shape of $\mu(p)$.

Based on recent applications [17,18,19,20,21] the static axial pressure on sliders of FP (and TFP) bearings are much less than 100 MPa and are not expected to exceed 100 MPa under earthquake loading. The parameters of (2) are therefore fit to the experimental data for axial pressures less than 100 MPa. Parameters a_p and h_p are set equal to 0.7 and 0.02, respectively, to define the shape of $\mu(p)$. For a very small value of $\tilde{\mu}_p$, (2) reduces to

$$\mu(p) = \mu_{p_o} \times 0.7^{(p - p_o)/50} \tag{3}$$

where all variables and parameters were defined previously. Figure 3 plots (3) with values of p_o and μ_{p_o} set equal to 10 MPa and 0.11, respectively. The curve matches the experimental data

well for axial pressures less than 100 MPa. For other liner materials, experiments should be conducted and the parameters of (2) fitted to that data.

2.3 Dependence of the coefficient of friction on temperature at the sliding surface

There are no direct measurements of the temperature dependence of the coefficient of friction because it is virtually impossible to measure temperature at the sliding surface while the slider is in motion. Measurements using a thermocouple installed below the sliding surface [10] can be used to indirectly measure temperature rise at the surface through convolution.

Constantinou et al. [3] present information on the reduction in the coefficient of friction with increasing temperature for the class of liners studied here. The coefficient decreases rapidly as the temperature at the sliding interface increases from -40°C to 20°C, and decreases more slowly thereafter and trends to a constant value for temperatures greater than 250°C. The relationship between coefficient of friction, $\mu(T)$, and temperature, T, can be described (e.g., [11]) by:

$$\mu(T) = \mu_{T_o} \times \left(\tilde{\mu}_T + (1 - \tilde{\mu}_T) a_T^{h_T (T - T_o)} \right) = \mu_{T_o} \times m \left(a_T^{h_T T} + n \right) \quad (4)$$

where μ_{T_o} is the high-velocity coefficient of friction at the reference temperature T_o, $\tilde{\mu}_T$ is the ratio of the coefficient of friction at high temperature (e.g., 250°C) to μ_{T_o}, a_T and h_T determine the rate of change in the coefficient of friction with temperature, and m and n are functions of a_T, h_T, $\tilde{\mu}_T$ and T_o.

For the purpose of this study, it is assumed that the ratios of the coefficients of sliding friction for T = -40°C, 20°C and 250°C are 3:2:1 for all values of sliding velocity and axial pressure, and T_o is set equal to 20°C. The ratio of the coefficients of friction at 20°C and 250°C of 2:1 recovers well the results of a displacement-controlled test on a single FP bearing [3]. The estimated peak temperature at the sliding surface at the end of 10 cycles of loading was 260°C; the coefficient of friction decreased by 50% during this experiment.

The shape parameters of (4), a_T and h_T, are set equal to 0.7 and 0.02, respectively, based on the available experimental data. With n = 0.4, $\mu(T)$ gives the desired ratios at the three temperatures. Finally, m is set equal to 0.79 so $\mu(T) = \mu(T_o)$ for $T = T_o$. The resulting expression to define the temperature dependence of friction is:

$$\mu(T) = 0.79 \mu_{T_o} \left(0.70^{T/50} + 0.40 \right) \quad (5)$$

The ratios of the coefficient of friction per (5) are 3.0:2.2:1.0 at the three temperatures, and very close to the target of 3:2:1. (The effect of these ratios on response is discussed later in the paper.)

2.3.1 Temperature at a monitoring point on the sliding surface

The temperature at a point on the sliding surface depends on the loading path (prior heating of the surface and its decay with time) and the instantaneous heat flux, which is a function of the

temperature at the sliding surface. At a monitoring location on the sliding surface, the temperature rise ΔT at time t is calculated using (6), which assumes a half space below the contact surface [3]:

$$\Delta T(t) = \frac{\sqrt{D}}{k\sqrt{\pi}} \int_0^t q(t-\tau) \frac{d\tau}{\sqrt{\tau}} \tag{6}$$

where D is the thermal diffusivity of stainless steel (comprising the concave sliding surface), k is thermal conductivity of stainless steel, τ is a time parameter that varies between 0 and t, and q is the heat flux. The half-space assumption is valid because the vertical penetration of heat into the concave plate is small by comparison with the plan dimensions of the bearing [5]. Based on [5], D and k are 4.44x10^{-6} m^2/s and 18 W/(m$^\circ$C), respectively. The instantaneous heat flux, $q(t)$, is

$$q(t) = \begin{cases} \mu(t)\, p(t) v(t) & \text{if } d \le r_{contact} \\ 0 \text{ otherwise} \end{cases} \tag{7}$$

where $\mu(t)$, $p(t)$ and $v(t)$ are the values of the coefficient of friction, axial pressure and velocity, respectively, d is the lateral displacement of the slider, and $r_{contact}$ is the radius of the slider (contact area). For ease of computation, the circular slider is replaced by a square of the same area. The temperature at a monitoring point increases as the slider passes over it due to the imposed heat flux and decreases towards ambient otherwise. Thermal radiation from the sliding surface is small and is ignored.

2.3.2 A representative temperature of the sliding surface for thermal calculations

The changes in the properties of the PTFE-type liner due to heating, and the consequent changes in the coefficient of friction are a function of the path of the slider on the sliding surface and the temperature on the sliding surface directly beneath the slider. Two methods to calculate a representative temperature for thermal calculations are investigated below, where one method is more computationally expensive than the other.

For the first and computationally more expensive method, temperature is tracked at a grid of uniformly distributed points on the sliding surface; an average value of the temperature at points directly below the slider is used for T in (5). Figure 4a shows the plan view of an FP bearing with a square grid of monitoring points and the orbit of the center of the slider, when the bearing is subjected to a ground motion. The sides of the equivalent square slider are oriented parallel to the two horizontal axes of the bearing. For the configuration shown in the panel, the average temperature at the two points directly below the slider is used in (5) to compute $\mu(T)$.

For the second method, the temperature at the center of the sliding surface is used in (5), which increases only when slider is directly above the center of the bearing and decreases

otherwise [3]. The sides of the equivalent square slider are oriented parallel and perpendicular to the line joining the centers of the slider and the sliding surface, as shown in Figure 4b.

Figure 5 shows the orbit of the center of the slider for an FP bearing with a sliding period of 3 s, a slider radius of 0.2 m, a Coulomb-type coefficient of friction of 0.06, and a static axial pressure of 50 MPa, subjected to ground motions 1 and 30 in the bin, respectively. The perimeter of the slider, located here at the center of the bearing, is shown dashed. It is evident from these two panels that the center of the sliding surface is the most traversed point on the sliding surface for these two ground motions.

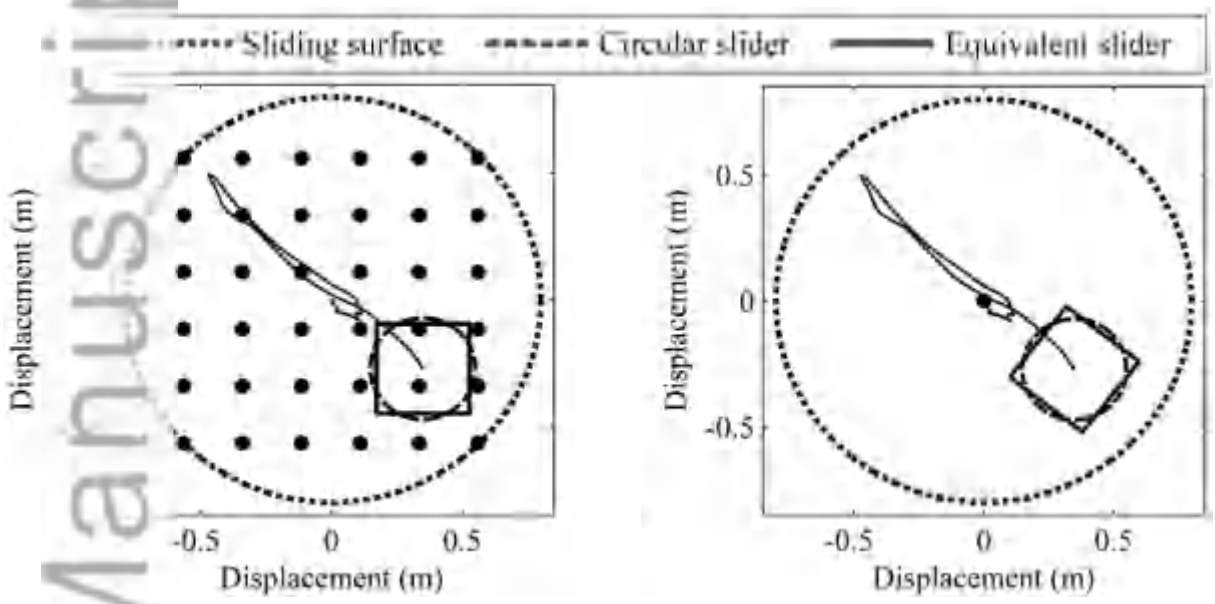

(a) Method 1 (b) Method 2

Figure 4. Calculating T for estimating $\mu(T)$

An FP bearing with a sliding period of 3 s, p_o = 50 MPa and μ_{ref} = 0.06 is analyzed for the 30 sets of ground motions of Section 1. Friction is described using the temperature-dependent friction model (equation (5)) with temperature calculated using the two methods. Two grid sizes are considered for the first method: 0.25 m and 0.15 m. Figure 6 presents the distributions of maximum displacement, where the displacement is assumed to follow a lognormal distribution. The median displacements calculated using the two grids of method 1 differ by 0.002 m. The difference in the median displacements calculated using the two methods is 0.037 m (0.563 m for method 1 and 0.600 m for method 2). The 99th percentile displacements are virtually identical. For the thirty ground motions, the minimum, mean and maximum differences in the peak displacement computed using the two methods are 0.002 m, 0.041 m, and 0.119 m, respectively. Considering these relatively small differences, the computationally more efficient second method is used hereafter.

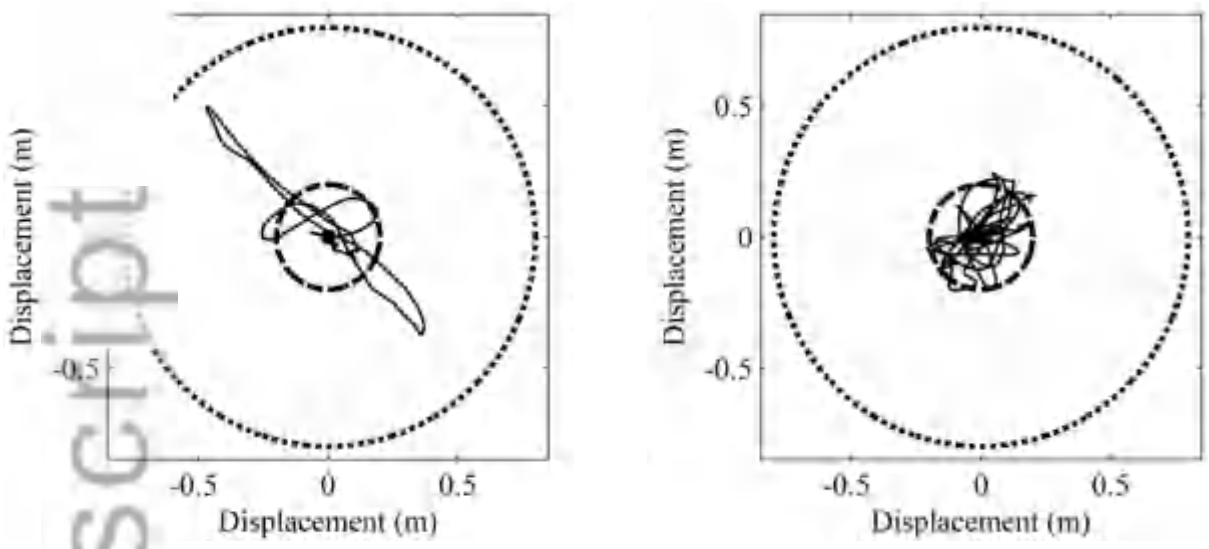

(a) Ground motion 1 (b) Ground motion 30

Figure 5. Orbit of the center of the slider of an FP bearing subjected to the ground motions

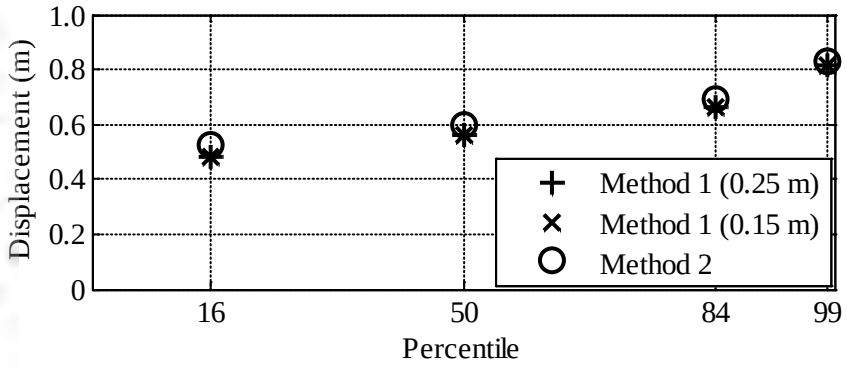

Figure 6. Distribution of maximum displacement of FP bearing with the temperature dependent coefficient of friction defined using different methods

2.4 Combined effect of velocity, pressure and temperature on friction

The right side of equations (1), (3) and (5) are the product of a reference coefficient of friction multiplied by factors accounting for velocity, pressure and temperature, respectively. In (1), $\mu_{\max}$ is the reference coefficient of friction at a very high sliding velocity. Similarly, in (3) and (5), μ_{p_o} and μ_{T_o} are the coefficient of friction at a reference axial pressure p_o and a reference temperature T_o, respectively. The factors accounting for the effect of velocity, k_v, axial pressure, k_p, and temperature, k_T, are given by the equations below, noting that are specific to the liner materials used in FP bearings in the United States:

$$k_v = 1 - 0.5e^{-100v} \tag{8}$$

$$k_p = 0.70^{(p-p_o)/50} \tag{9}$$

$$k_T = 0.79\left(0.70^{T/50} + 0.40\right) \tag{10}$$

where all the terms have been defined previously.

The reference coefficient of friction μ_{ref} is defined as the coefficient of friction at a bearing pressure p_o, measured at a high velocity of sliding for a temperature at the sliding surface of T_o (=20˚C). The coefficient of friction, adjusted for the effects of axial pressure, temperature and velocity, $\mu(p,T,v)$, is then obtained as the product of the reference coefficient of friction and the three factors:

$$\mu(p,T,v) = \mu_{ref}\left(k_p k_T k_v\right) \tag{11}$$

This method to consider the pressure, temperature and velocity dependences of the coefficient of friction is incorporated in an OpenSees [7] element for an FP bearing.

Figure 7 shows the variation in the coefficient of sliding friction with sliding velocity, axial pressure and temperature at the sliding surface. Figure 7a plots the coefficient of friction against temperature for three values of sliding velocity (=1 m/s, 0.01 m/s and 0 m/s) using equations (8), (10) and (11), with μ_{ref} = 0.06, T_o = 20°C and k_p = 1. Figure 7b plots the coefficient of friction against axial pressure using equations (8), (9) and (11) with μ_{ref} = 0.06, p_o = 10 MPa and k_T = 1 (or T = 20°C), for three values of sliding velocity. If the temperature at the sliding surface rises from 20°C to a maximum of 250°C, the high-velocity coefficient of friction will decrease from 0.060 to 0.030 for a constant axial pressure. Similarly, if the axial pressure on the bearing ranges between 2 MPa and 18 MPa, the high-velocity coefficient of friction will vary between 0.064 and 0.057. This variation is assumed to be independent of that due to temperature change. The small-velocity coefficients of friction are one half the high-velocity coefficients for all values of temperature and pressure. The transition from the small-velocity coefficient of friction to the high-velocity coefficient of friction is sharp and the value of k_v is close to 1.0 during strong shaking.

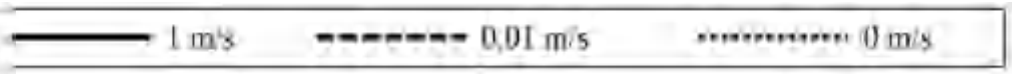

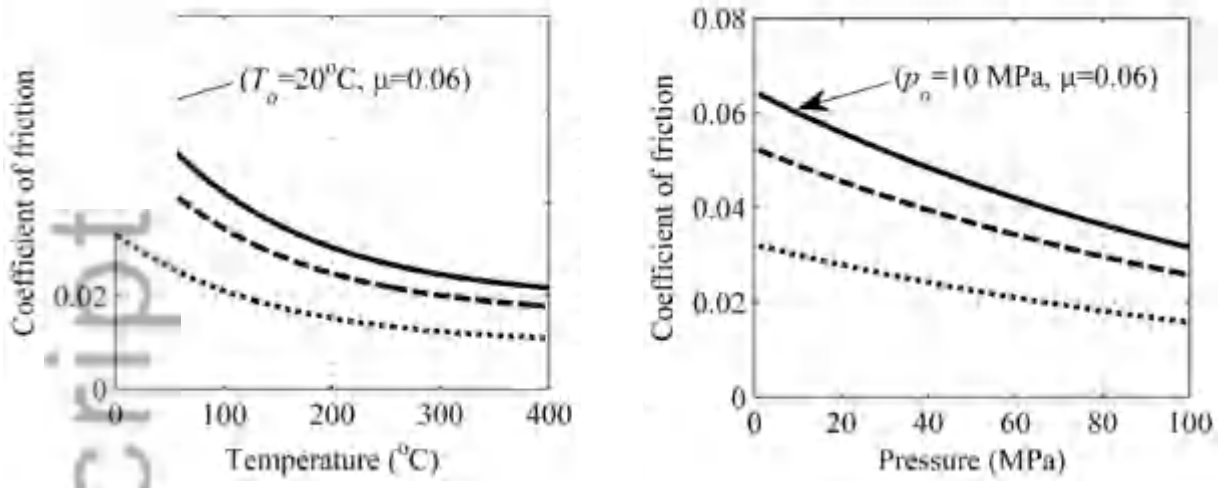

(a) Friction vs. temperature (b) Friction vs. pressure

Figure 7. Variation in the coefficient of sliding friction with sliding velocity, axial pressure and temperature at the sliding surface

2.5 Validation of numerical models

The numerical approach described above is validated using two experiments. The first experiment is reported in [3]: an FP bearing with the radius of curvature of 4 m and a static axial pressure of 30.8 MPa, subjected to a reversed cyclic displacement history with a frequency of 0.6 Hz and an amplitude of 0.250 m. The velocity of sliding fluctuated between -1.190 m/s and 0.924 m/s during the experiment. The radius of the contact area was 0.260 m. Figure 8a shows the experimentally recorded force-displacement history as digitized from [3]. The reduction in the coefficient of friction is evident from the change in the level of shearing force at a given displacement with an increasing number of cycles. The force-displacement response is simulated using two friction models: 1) pressure, temperature and velocity dependent, *p-T-v*, and 2) Coulomb. The high-velocity coefficient of friction at the beginning of experiment was 0.05. The first three cycles of the simulated histories of normalized force (ratio of horizontal to vertical force) using the two friction models are compared with the experimental history in Figure 8a. Figure 8b plots the recorded and simulated normalized force histories for the three cycles. The force-displacement history obtained using the *p-T-v* model simulates the experimentally recorded history much better than the Coulomb model. Figure 8c plots the force-displacement response of the bearing in the tenth cycle of loading. The *p-T-v* model recovers the recorded response well unlike the Coulomb model. The high-velocity coefficient of friction in the tenth cycle is approximately one half of that at the beginning of the experiment. The maximum temperature at the center of the bearing computed using the *p-T-v* model was 260°C.

The second experiment used to validate the numerical model is an earthquake simulator test of a seven story steel structure that was seismically isolated using eight FP bearings. The static axial pressure on each of the bearing was approximately 124 MPa. The radius of curvature of the bearings was 0.248 m. The high-velocity coefficient of friction of the bearings was

estimated from the observed force-displacement response to be 0.07. Earthquake shaking was imposed along one horizontal axis only. Details on the structure, bearings, ground motion and recorded response are presented in [16,22]. The displacement history of the isolation system is simulated here, noting that the recorded displacement histories for the eight bearings were virtually identical. A single FP bearing with static axial pressure of 124 MPa, static axial load of 35 kN (load on an internal bearing considered in [22]), radius of curvature of 0.248 m and a reference coefficient of friction of 0.07 is analyzed. The variation in axial pressure on the slider due to the rocking response of the superstructure is ignored, which is appropriate when comparing with measured system responses. Figure 9 plots the experimentally recorded displacement history of the isolation system and those computed using the two friction models: *p-T-v* and Coulomb. The measured and simulated peak positive displacements are 0.052 m, 0.047 m (*p-T-v*) and 0.038 m (Coulomb). The corresponding peak negative displacements are 0.052 m, 0.060 m, and 0.051 m.

On the basis of these comparisons of experimentally measured and numerically predicted displacement and force responses, the unified numerical model of Section 2.4 is validated.

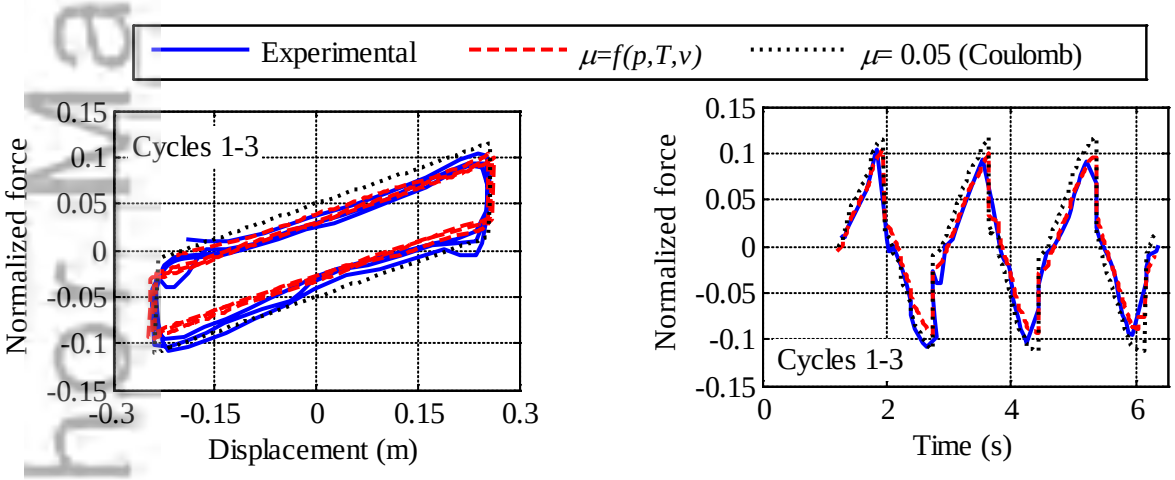

(a) Normalized force-displacement history

(b) Normalized force history

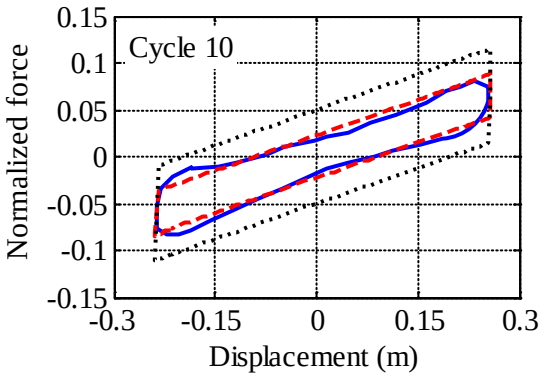

(c) Normalized force-displacement history

Figure 8. Experimental [3] and simulated normalized force-displacement histories of an FP bearing

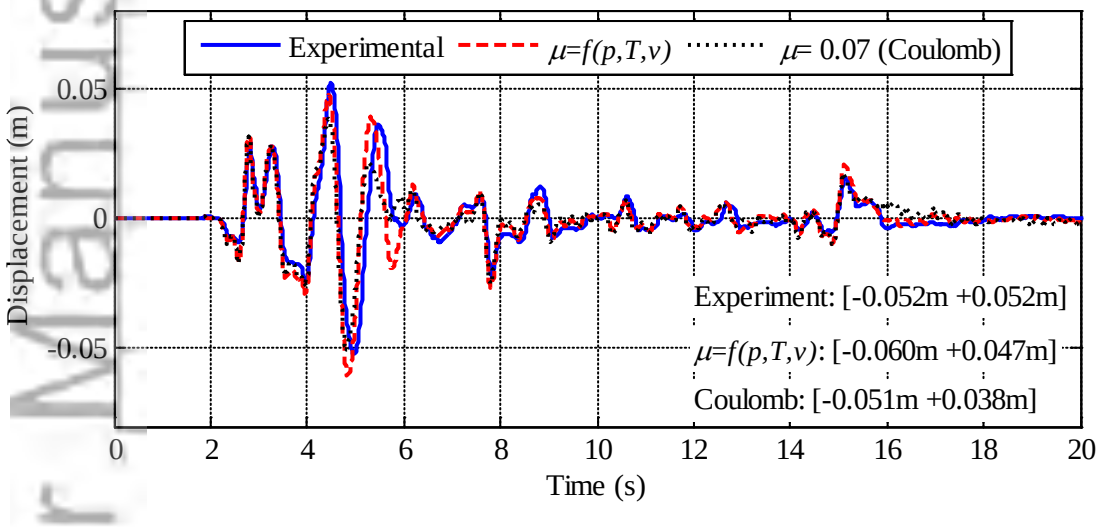

Figure 9: Experimentally recorded [16,22] and simulated displacement histories of an isolation system comprising FP bearings

3. RESPONSE-HISTORY ANALYSIS AND RESULTS

3.1 Numerical models

Response-history analyses are performed to better understand the influence of the factors that affect the coefficient of sliding friction on the displacement response of sliding isolation systems. FP bearings with a range of geometrical and material properties, and two levels of axial pressure are subjected to the 30 sets of ground motions (GMs) of Section 1. Bearings with a sliding period of 2 s, 3 s and 4 s, μ_{ref} of 0.06, and p_o of 10 MPa and 50 MPa are analyzed. The static axial

pressure p_o is due to gravity loadings. The pressure on the slider changes continuously during the simulations due to the vertical component of ground motion by up to ±70%. The pressure dependence of friction is described by two curves, obtained from (9) for static axial pressures of 10 MPa and 50 MPa, covering the range of recent applications of FP bearings. The slider radius is 0.200 m. Analyses were performed with friction described by the five models of Table 1.

3.2 Coefficient of friction

Figure 10 presents the coefficient of friction averaged over the duration of strong shaking for FP bearings with sliding periods of 2 s, 3 s and 4 s, a reference coefficient of friction of 0.06, static axial pressures of 10 MPa and 50 MPa, and friction at the sliding surface defined by the five friction models of Table 1, subjected to the 30 sets of ground motions of Section 1. The durations of strong shaking for the ground motions (greater of the values in two horizontal directions [23]) range between 6.6 s (GM20) and 28.2 s (GM29) with an average 14.2 s. The responses can be parsed into two groups depending on whether the friction model includes the effects of temperature. For example, for the 3 s bearing with a static axial pressure of 10 MPa subjected to GM29 (Figure 10b), the average values of the coefficient of friction are 0.060, 0.060 and 0.059 if the friction model is Coulomb (Model 1), pressure-dependent (Model 2) and velocity-dependent (Model 4), respectively, whereas the values are 0.050 and 0.050, respectively, if the friction is assumed to vary only with temperature (Model 3) and varies with pressure, temperature, and velocity (Model 5). The heating effects are much more significant if the static axial pressure is increased in Figures 10d, 10e and 10f. As can be seen in Figure 10e for the 3 s bearing with a static axial pressure of 50 MPa, when subjected to GM29, the average values of the coefficient of friction over the duration of strong shaking are 0.06, 0.06 and 0.059, when the friction model ignores temperature (Models 1, 2 and 3, respectively), and 0.035 and 0.034 for Models 3 and 5, respectively, which include the effects of temperature.

Table 1. Friction models considered in the study

	Friction model	**Notation**
Model 1	Coulomb	μ = Coulomb
Model 2	Pressure dependent	$\mu = f(p)$
Model 3	Temperature dependent	$\mu = f(T)$
Model 4	Velocity dependent	$\mu = f(v)$
Model 5	Pressure, temperature and velocity dependent	$\mu = f(p,T,v)$

For the 3 s bearing with a static axial pressure of 10 MPa subjected to GM29, the coefficient of friction averaged over the duration of strong shaking is 17% smaller if the temperature dependence of friction is considered. The difference is 42% for a static axial pressure of 50 MPa. Averaged across all 30 sets of ground motions, the differences are 13% and 34% for static axial pressures of 10 MPa and 50 MPa, respectively. The differences for the 2 s bearings are 18% and 42%, and 12% and 32% for the 4 s bearings, if the static axial pressures

are 10 MPa and 50 MPa, respectively. The heating effects are more pronounced for the bearings with a smaller sliding period, which is expected because the displacements in these bearings is less than those in the 3 s and 4 s bearings, which concentrates the heat flux on a smaller area of the sliding surface, resulting in a greater increase in temperature and a greater change in the coefficient of friction.

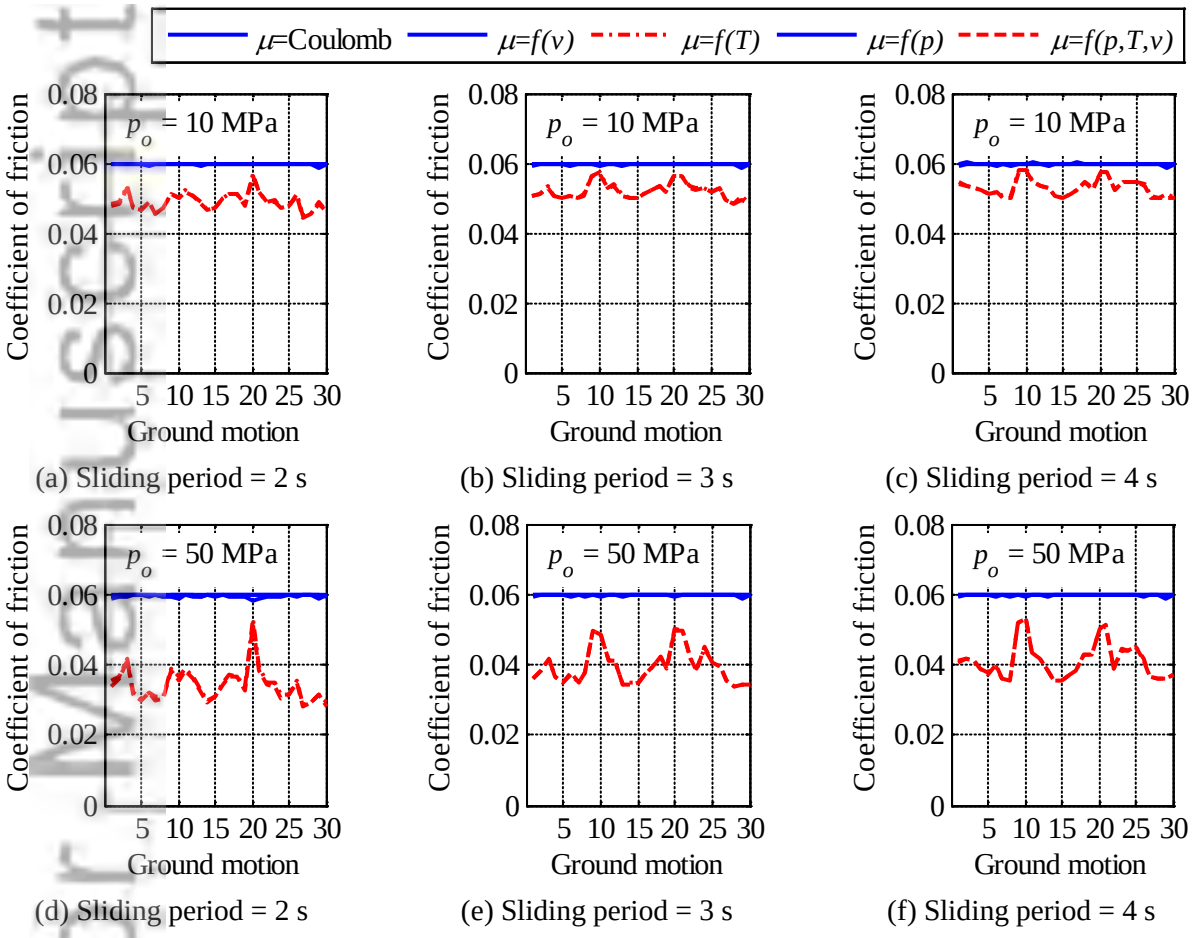

(a) Sliding period = 2 s (b) Sliding period = 3 s (c) Sliding period = 4 s

(d) Sliding period = 2 s (e) Sliding period = 3 s (f) Sliding period = 4 s

Figure 10. Coefficient of friction averaged over the duration of strong shaking for bearings with different geometrical properties and static axial load

Figure 11a presents the history of the coefficient of friction for the bearing with a sliding period of 3 s, reference coefficient of friction of 0.06 and static axial pressure of 50 MPa, subjected to GM29. Two friction models are considered: Coulomb (Model 1) and *p-T-v* (Model 5). Figures 11b, 11c and 11d present histories of k_p, k_T and k_v, respectively. The high frequency changes in the pressure factor are due to the vertical ground motion, ranging between 0.8 and 1.3, with an average of 1.0, over the duration of strong shaking (between 6 s and 34 s).

The temperature factor varies between 0.5 and 0.8 in the duration with an average of 0.6. The velocity factor varies from 0.5 to 1.0, with an average value of 1.0 during strong shaking.

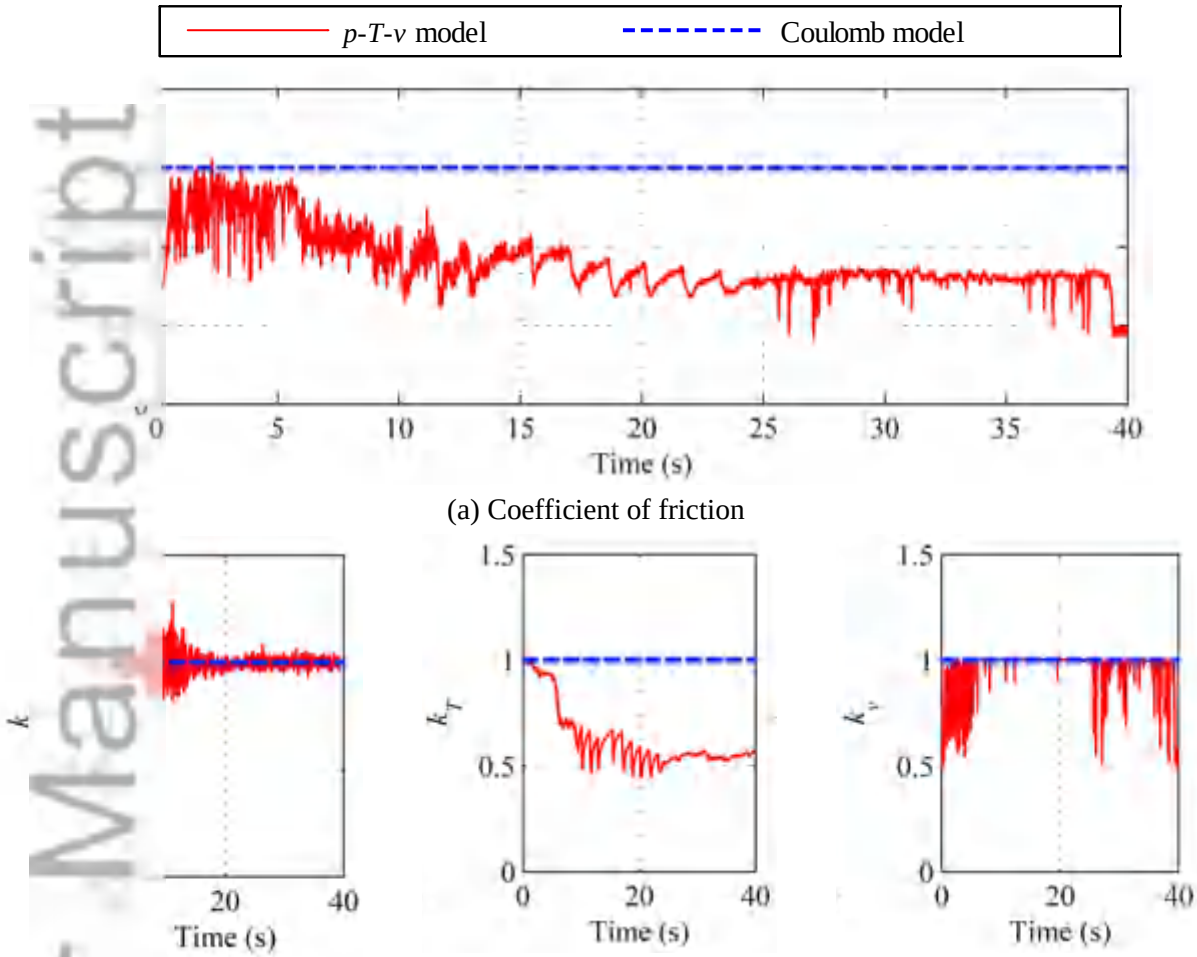

(a) Coefficient of friction

(b) Pressure factor (c) Temperature factor (d) Velocity factor

Figure 11. Histories of coefficient of friction and the factors defining the dependence of the coefficient of friction on axial pressure, temperature and velocity; GM29

3.3 Force-displacement history

The force-displacement histories of FP bearings with a sliding period 3 s, reference coefficient of friction 0.06, static axial pressures of 10 MPa and 50 MPa, friction behavior described by Model 1 (Coulomb) and Model 5 (*p-T-v*), and subjected to GM30, are presented in Figure 12. The maximum displacement for Model 1 is 0.276 m: the smallest for the 30 motions. Heating effects, and consequently the choice of friction model, are expected to be most important when the maximum displacement is small, although this is likely of limited practical importance. For a static axial pressure of 10 MPa, the maximum displacement increases from 0.246 m (Figure 12a,

Coulomb) to 0.311 m (Figure 12c, *p-T-v*). For the greater static axial pressure of 50 MPa, the maximum displacement increases from 0.246 m (Figure 12b, Coulomb) to 0.483 m (Figure 12d, *p-T-v*). The reduction in the coefficient of friction is evident by comparing the shearing forces in Figures 12a and 12c, and 12b and 12d.

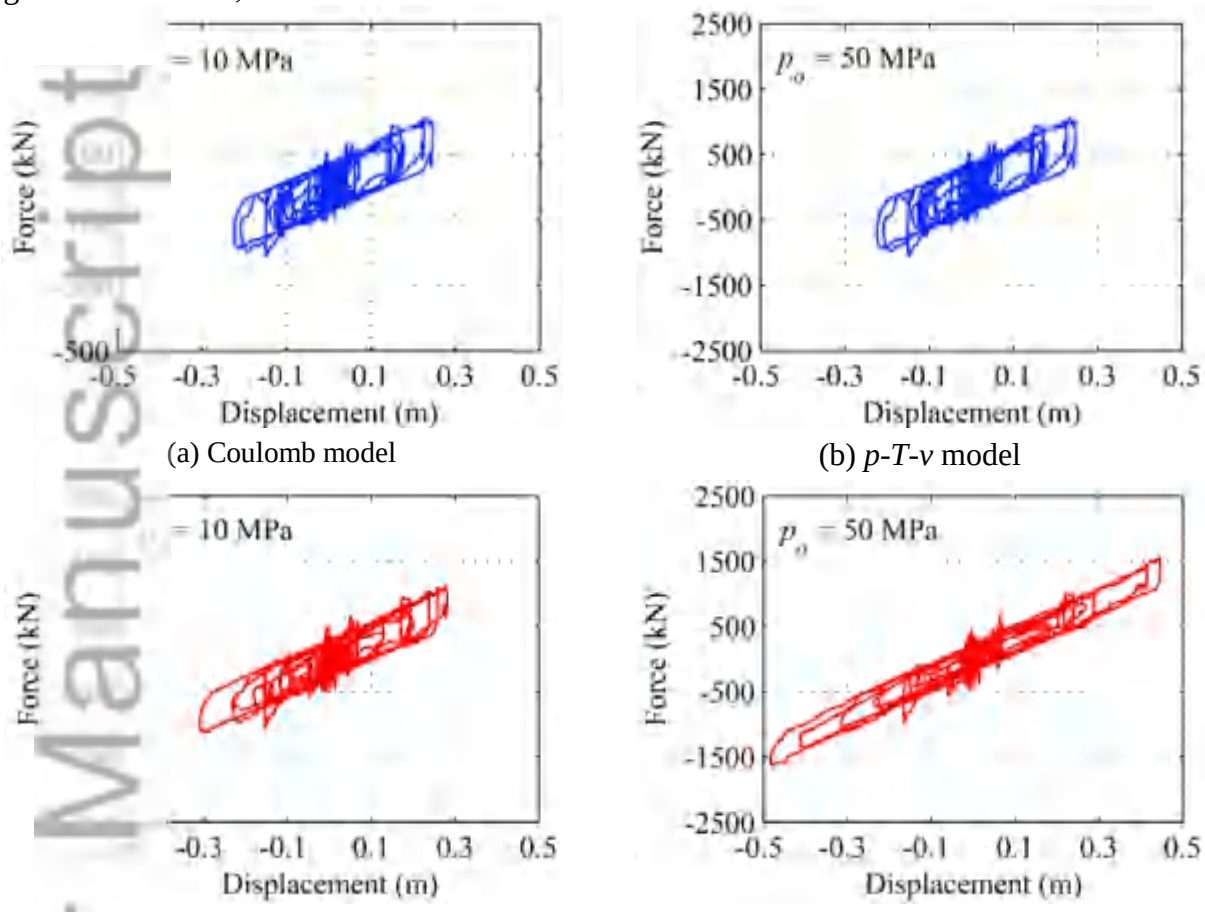

(a) Coulomb model (b) *p-T-v* model

(c) Coulomb model (d) *p-T-v* model

Figure 12. Force-displacement histories of an FP bearing in Y direction with sliding isolation period of 3 s and reference coefficient of friction 0.06, subjected to GM30

3.4 Maximum displacement

Figure 13 presents the 16th, 50th, 84th and 99th percentiles of maximum displacement for FP bearings with sliding isolation period of 2 s, 3 s and 4 s, static axial pressure of 10 MPa and 50 MPa, the five friction models of Table 1, subjected to the 30 sets of ground motions of Section 1. The distributions are assumed to be lognormal, which is supported by goodness-of-fit tests (Chi-square, Lilliefors and Jarque-Bera) that showed for 90% of the combinations of sliding period, static pressure and friction model, that the log of the 30 values of maximum displacement distributed normally with 5% significance.

Figures 13a, 13b and 13c present results for a static axial pressure of 10 MPa and 2 s, 3 s and 4 s bearings, respectively. The choice of friction model does not substantially affect the distributions of maximum displacement response. Figures 13d, 13e and 13f present companion results for a static axial pressure of 50 MPa. The choice of friction model is important in these cases because more heat is generated due to the greater axial pressure. For the static axial pressure of 50 MPa, the effect of the choice of friction model is less important, measured in terms of a percentage increase in displacement, for the higher percentiles.

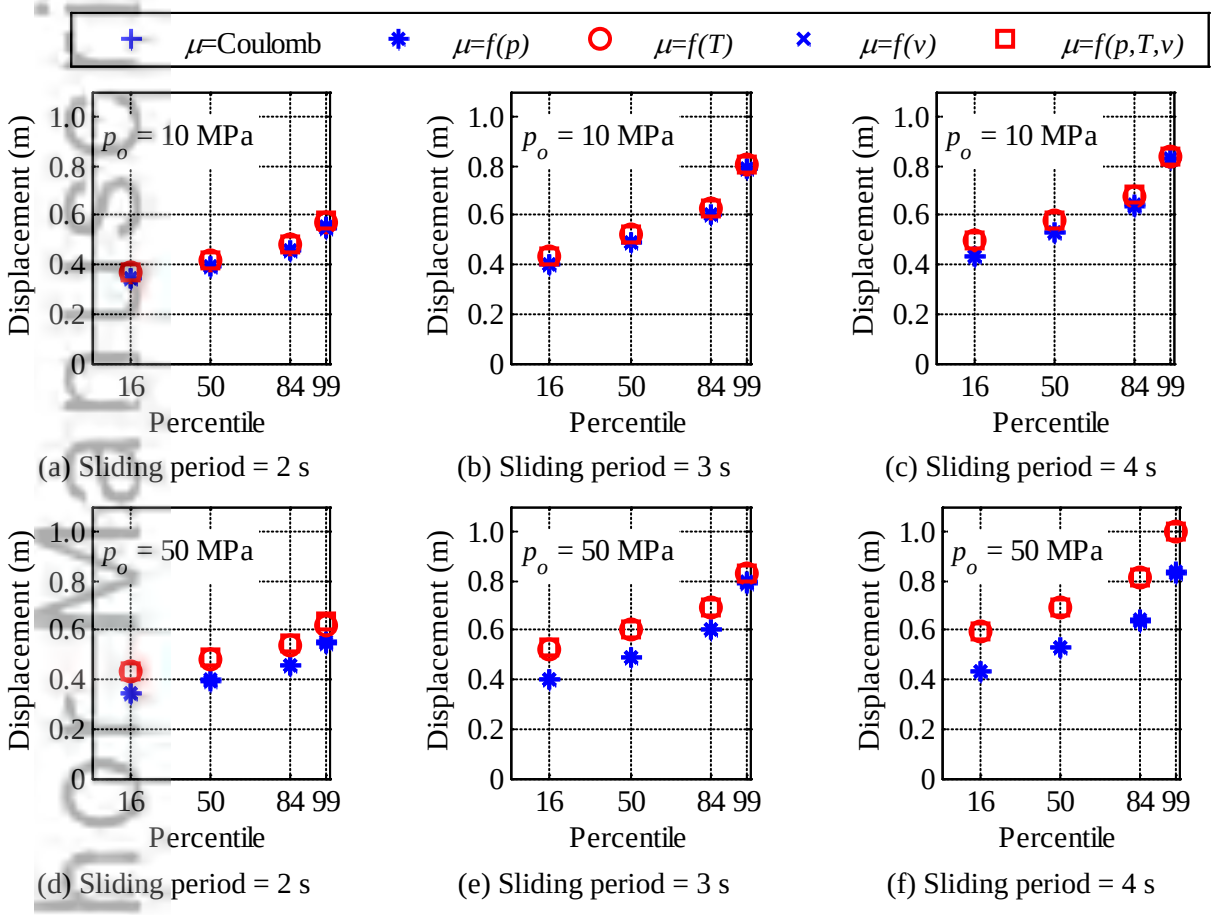

Figure 13. Distribution of displacement demand

3.4.1 Ratios of the coefficient of friction at different temperatures

The ratio of the coefficient of friction at -40°C, 20°C and 250°C was set in Section 2.3 to 3:2:1. The impact of this assumption is studied here by changing the ratio in the temperature range from 20°C to 250°C. A ratio of 2:0.9 is achieved using (10) at these two temperatures. Two other

ratios, 2:0.5 and 2:1.5, are considered. The parameters a_T and h_T of (4) are set to 0.7 and 0.02, respectively. The remaining two parameters, m and n, are selected to achieve the target coefficients of friction at the two temperatures. Table 2 lists the expressions to define the three models: TM1, TM2 and TM3. Figure 14 plots the temperature factors for the three models along with that for the Coulomb model.

FP bearings with a sliding period of 3 s, p_o of 10 MPa and 50 MPa, and μ_{ref} of 0.06 are subjected to the 30 sets of ground motions of Section 1. Figure 15a presents the distribution of maximum displacement response of the bearing with a static axial pressure of 10 MPa, for friction at the sliding surface described by the Coulomb model and the three temperature-dependent friction models of Table 2. The distribution of displacement demand is not significantly affected by the choice of friction model for this static axial pressure, as observed previously. The choice of friction model is much more important at the static axial pressure of 50 MPa (Figure 15b). Analysis using the temperature-dependent models predicts greater displacements than that using the Coulomb model, with smaller percentage differences in the displacements at the higher percentiles. These calculations emphasize the need for appropriate characterization of the relationship between the coefficient of friction and temperature, which may be substantially different for liner materials different from those investigated here.

Table 2. Expressions to define the temperature dependence of friction

Model	**Expression**	$\mu_{20°C} : \mu_{250°C}$
TM1 (10)	$k_T = 0.79\left(0.70^{T/50} + 0.40\right)$	2 : 0.9
TM2	$k_T = 1.08\left(0.70^{T/50} + 0.06\right)$	2 : 0.5
TM3	$k_T = 0.36\left(0.70^{T/50} + 1.9\right)$	2 : 1.5

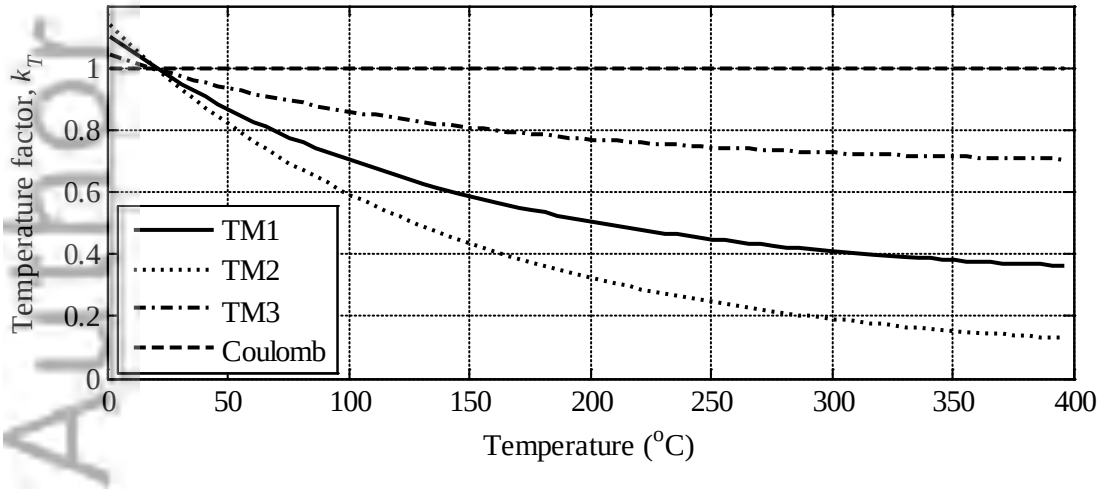

Figure 14. Effect of choice of temperature model

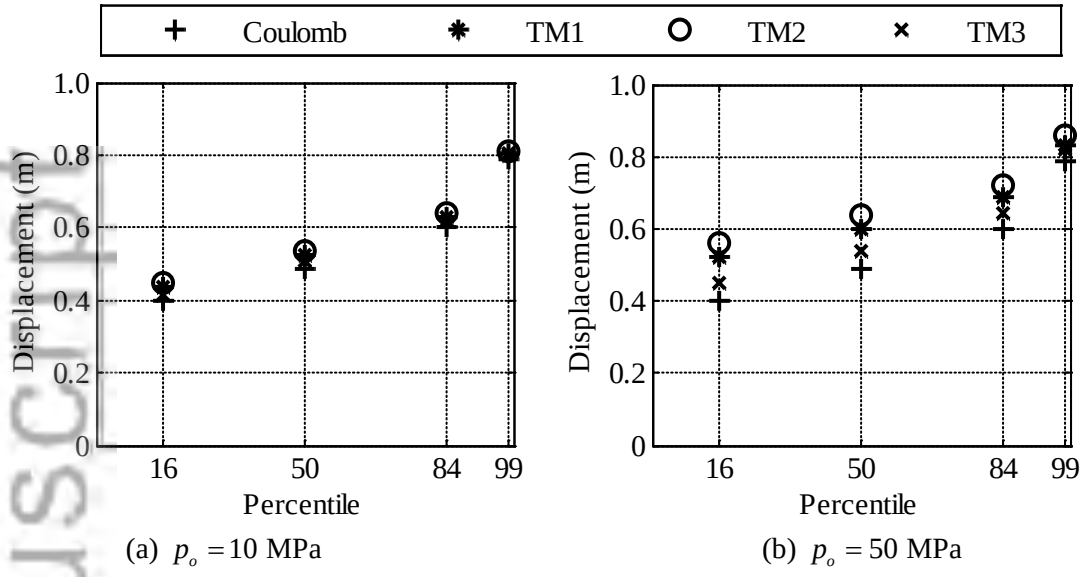

Figure 15. Maximum displacements of 3 s bearings with Coulomb friction and the temperature-dependent friction models of Table 2

3.5 *Maximum temperature at the sliding surface*

Figure 16a presents the 16th, 50th, 84th and 99th percentiles of maximum temperature at the center of a bearing with a sliding period of 2 s and a static axial pressure of 10 MPa, noting that this calculation is only relevant if heating effects are to be included in the model. A lognormal distribution of the maximum temperature is assumed. (The peak temperatures distribute lognormally for 70% to 100% of the combinations of Section 3.4 for the three goodness-of-fit tests). The effect of choice of friction model on temperature at the center of the bearing is insignificant for the smaller static axial pressure of 10 MPa. For the static axial pressure of 50 MPa, ignoring the temperature dependence of friction will overestimate the temperature increase because the reduction in the coefficient of friction and consequently the heat flux, which accompanies the increase in temperature, is not accounted for.

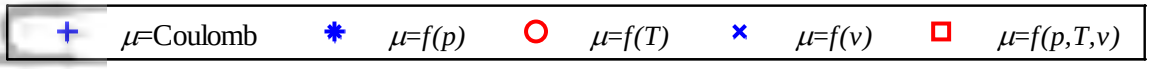

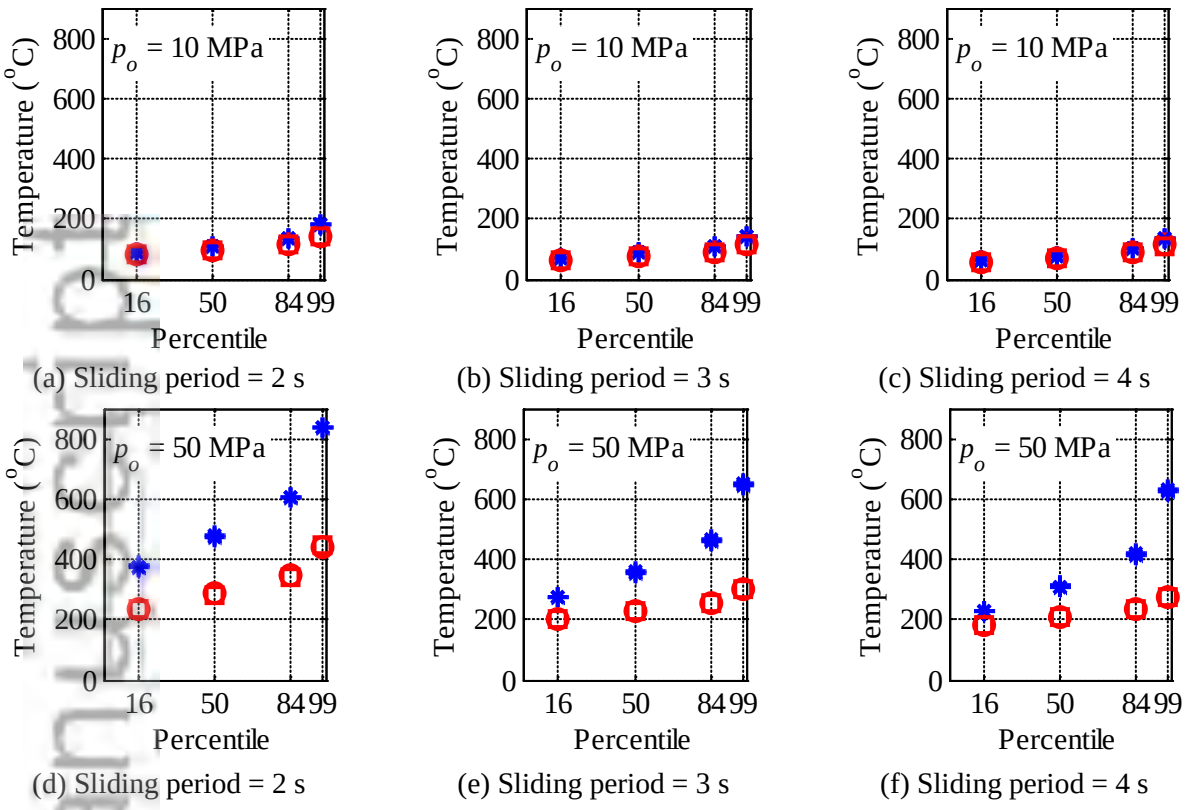

Figure 16. Distributions of maximum temperature

3.6 Floor response spectra

Floor response spectra are routinely used for the design of structures, systems and components in safety-related nuclear structures, and are being used for this purpose in mission-critical buildings. The effect of choice of friction model on floor spectra is investigated here using the absolute acceleration response of the slider in one horizontal direction. Figure 17 presents data for bearings with sliding periods of 2 s, 3 s and 4 s, static axial pressures of 10 MPa and 50 MPa, and a reference coefficient of friction of 0.06, subjected to the 30 sets of ground motions of Section 1. The use of a lognormal distribution for the spectral ordinates at a given period is supported by goodness-of-fit tests, as described previously.

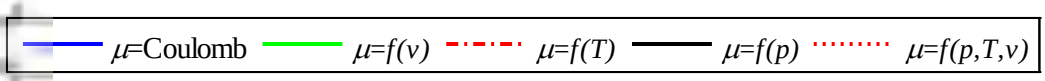

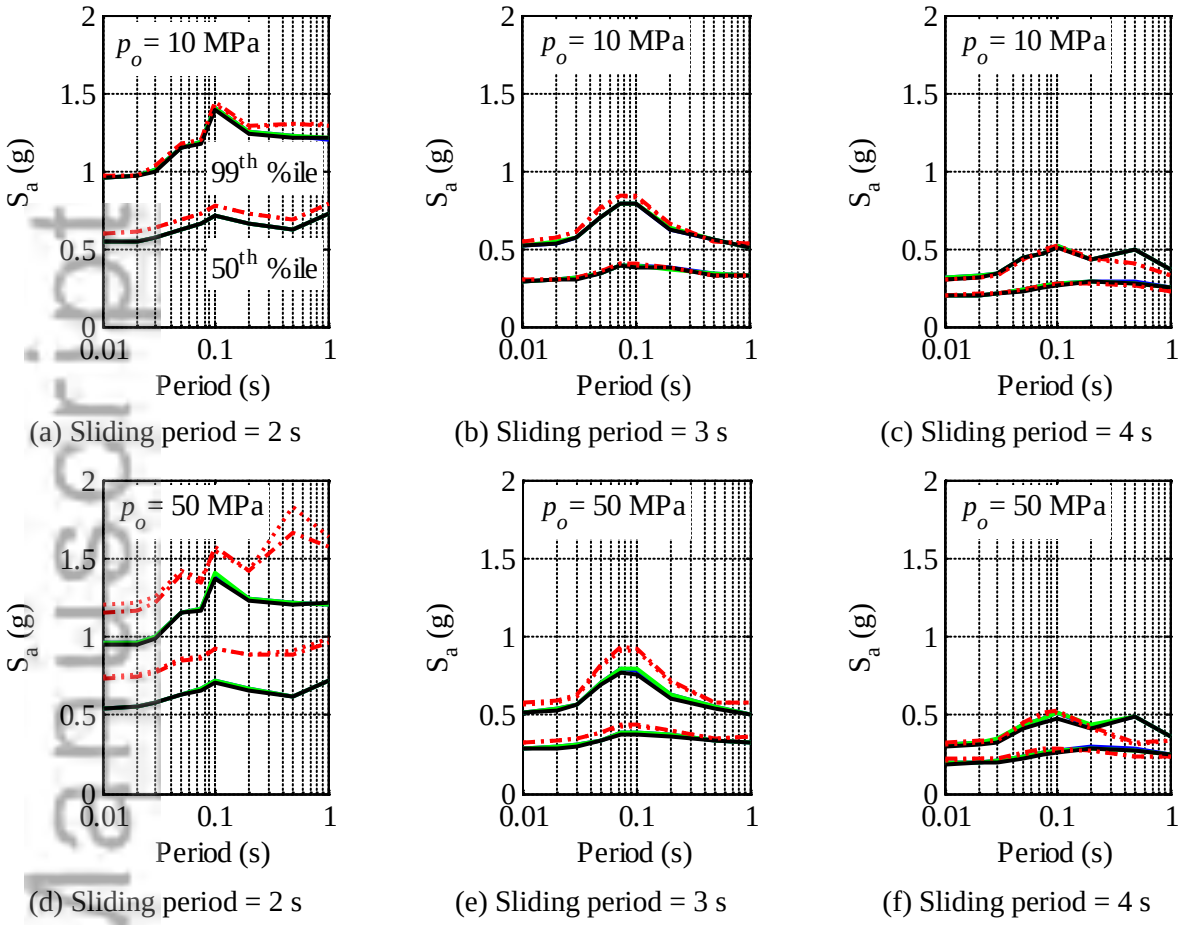

(a) Sliding period = 2 s (b) Sliding period = 3 s (c) Sliding period = 4 s

(d) Sliding period = 2 s (e) Sliding period = 3 s (f) Sliding period = 4 s

Figure 17. 50th and 99th percentiles of 5% damped floor response spectral ordinates in the X direction for bearings with sliding period of 2 s, 3 s and 4 s

Figures 17a, 17b and 17c present the 5% damped 50th and 99th percentile floor spectral ordinates for the 2 s, 3s and 4s bearings, respectively, with a static pressure of 10 MPa. The choice of friction model does not significantly affect the spectral ordinates at this static axial pressure. The spectral ordinates are considerably smaller for the longer sliding periods: 3s and 4s. Heating effects are more evident at the higher static axial pressure of 50 MPa, especially for the 2 s bearing (Figure 17d). The spectral ordinates are generally smaller if the friction model ignores the effects of heating but no definitive conclusions can be drawn. The spectral ordinates are not altered materially if either the velocity dependence and/or the pressure dependence of friction are considered.

4. SUMMARY AND CONCLUSIONS

A unified framework to incorporate the complex interdependence of the coefficient of sliding friction, axial pressure, sliding velocity and temperature at the sliding surface into a response-history analysis of a structure isolated with spherical sliding bearings is presented. Suitable assumptions are made to decouple the dependence of axial pressure and velocity on the coefficient of friction. Expressions to define the relationship between the coefficient of friction and axial pressure, sliding velocity, and temperature at the sliding surface are proposed based on available experimental data. A procedure to compute temperature at the sliding surface during a response-history analysis is described. Response-history analyses are performed using ground motions for the site of the Diablo Canyon Nuclear Generating Station to understand the influence of the three factors on maximum isolator displacement and floor response spectra.

The importance of the choice of friction model is highly dependent on the static pressure on the slider. For the single-concave sliding isolator considered here, constructed with PTFE-based composite materials, and using ground motions consistent with a region of high seismic hazard, the importance is low if the static pressure is relatively small (say 10 MPa) and high if the static pressure is significant (say 50 MPa). A friction model that ignores the effects of temperature rise may underestimate the median (84^{th}, 99^{th}) maximum displacement by 10% (5%, 5%) and 30% (25%, 20%), for static axial pressures of 10 MPa and 50 MPa, respectively. Floor spectral ordinates can be significantly affected by the choice of friction model if the static axial pressure on the slider is significant and sliding period of the bearing is short, with the effect of temperature being much greater than the effects of pressure and sliding velocity.

The effect of temperature rise on the sliding surface of a single concave bearing should be considered in the calculations of distributions of isolator displacement and the development of floor response spectra. The impact will vary by the response quantity of interest, the percentile sought, the static (gravity) pressure on the slider, the liner material used, and the ground motions adopted for analysis. For the calculation of isolator displacements, and for the liner material studied here, the effects of changes in velocity and axial pressure over the course of an earthquake on the coefficient of sliding friction are small and may not need to be included in a friction model. The pressure dependence of the coefficient of friction may be important if the rocking (overturning) response of the isolated structure is significant and/or the vertical shaking is intense, but very large earthquake-induced changes in vertical load (axial pressure) may result in tensile forces, which cannot be resisted by the FP bearing in the configuration assumed in this study.

ACKNOWLEDGEMENTS

This research project is supported by a grant to MCEER and the University at Buffalo from the United State Nuclear Regulatory Commission and the Lawrence Berkeley National Laboratory (LBNL). This financial support is gratefully acknowledged. The authors thank Dr. Robert Budnitz of LBNL who has advised the research team on technical matters and managed the

project, and Professor Yin-Nan Huang of National Taiwan University who provided the ground motion histories. The authors thank Dr. Shawn Matott of the Center for Computational Research (CCR) at the University at Buffalo for help in performing computations on the Linux based cluster.

5. REFERENCES

1. Constantinou MC, Tsopelas P, Kasalanati A, Wolff ED. Property modification factors seismic isolation bearings. University at Buffalo, Buffalo, NY, 1999. Report No. MCEER-99-0012.
2. Thompson ACT, Whittaker AS, Fenves GL, Mahin SA. Property modification factors for elastomeric seismic isolation bearings. *Proceedings, Twelfth World Conference on Earthquake Engineering*, Auckland, New Zealand, January 30-February 4, 2000.
3. Constantinou MC, Whittaker AS, Kalpakidis Y, Fenz DM, Warn GP. Performance of seismic isolation hardware under service and seismic loading. Multidisciplinary Center for Earthquake Engineering Research, Buffalo, NY, 2007. Report No. MCEER-07-0012.
4. Huang Y-N, Whittaker AS, Kennedy RP, Mayes RL. Assessment of base-isolated nuclear structures for design and beyond-design basis earthquake shaking. Multidisciplinary Center for Earthquake Engineering Research, Buffalo, NY, 2009. Report No. MCEER-09-0008.
5. Constantinou M, Mokha A, Reinhorn A. Teflon bearings in base isolation II: Modeling. *Journal of Structural Engineering* 1990; **116**(2): 455-474.
6. Computers and Structures Incorporated SAP2000 v. 15.2.1. 2013, Berkeley, California.
7. Pacific Earthquake Engineering Research (PEER) Center. Open System for Earthquake Engineering Simulation v. 2.4.3. 2014, Berkeley, California.
8. Constantinou MC, Tsopelas P, Kim Y-S, Okamoto S. NCEER-Taisei Corporation research program on sliding seismic isolation systems for bridges: Experimental and analytical study of a Friction Pendulum System (FPS). National Center for Earthquake Engineering Research, Buffalo, NY, 1993. Report No. NCEER-93-0020.
9. Tsopelas PC, Constantinou MC, Reinhorn AM. 3D-BASIS-ME: Computer program for nonlinear dynamic analysis of seismically isolated single and multiple structures and liquid storage tanks. National Center for Earthquake Engineering Research, Buffalo, NY, 1994. Report No. NCEER-94-0010.
10. Wolff E. Frictional heating in sliding bearings and an experimental study of high friction materials. *MS Dissertation*, University at Buffalo, State University of New York, Buffalo, NY 1999.
11. Sarlis AA, Constantinou MC. Model of Triple Friction Pendulum bearing for general geometric and frictional parameters and for uplift conditions. Multidisciplinary Center for Earthquake Engineering Research, Buffalo, NY, 2013. Report No. MCEER-13-0010.
12. Mokha A, Constantinou MC, Reinhorn AM. Teflon bearings in aseismic base isolation: Experimental studies and mathematical modeling. National Center for Earthquake Engineering Research, Buffalo, NY, 1988. Report No. NCEER-88-0038.

13. Fenz DM, Constantinou MC. Behaviour of the double concave Friction Pendulum bearing. *Earthquake Engineering & Structural Dynamics* 2006; **35**(11): 1403-1424. DOI: 10.1002/eqe.589.
14. Fenz DM, Constantinou MC. Modeling Triple Friction Pendulum bearings for response-history analysis. *Earthquake Spectra* 2008; **24**(4): 1011. DOI: 10.1193/1.2982531.
15. Zayas VA, Low SS, Mahin SA. The FPS earthquake resisting system experimental report. Earthquake Engineering Research Center, Berkeley, California, 1987. Report No. UCB/EERC-87/01.
16. Al-Hussaini TM, Zayas VA, Constantinou MC. Seismic isolation of multi-story frame structures using spherical sliding isolation systems. National Center for Earthquake Engineering Research, Buffalo, NY, 1994. Report No. NCEER-94-0007.
17. Mokha AS, Amin N, Constantinou MC, Zayas V. Seismic isolation retrofit of large historic building. *Journal of Structural Engineering* 1996; **122**(3): 298-308.
18. Zayas VA, Low S, Mokha AS, Imbsen RA. Seismic isolation of Benicia-Martinez Bridge. *Proceedings, Structures 2001*, Washington D.C., May 21-23, 2001.
19. Zekioglu A, Huseyin, Erkus B. Performance-based seismic design of a large seismically isolated structure: Istanbul Sabiha Gokcen International Airport Terminal Building. *Proceedings, SEAOC 2009,* San Diego, California, September, 2009.
20. Fenz DM, Seed R, Slatnick S, Stewart HR, Constantinou MC. Development of performance-based testing specifications for the Arkutun-Dagi Friction Pendulum bearings. *Proceedings, Arctic Technology Conference*, Houston, Texas, February 7-9, 2011.
21. Sarkisian M, Lee P, Hu L, Doo C, Zayas V, Constantinou M, Bachman R. Property verification of Triple Pendulum™ seismic isolation bearings. *Proceedings, 20th Analysis & Computational Specialty Conference, Structures Congress 2012*, Chicago, Illinois, March 29-31, 2012.
22. Scheller J, Constantinou MC. Response history analysis of structures with seismic isolation and energy dissipation systems: Verification examples for program SAP2000. Multidisciplinary Center for Earthquake Engineering Research, Buffalo, NY, 1999. Report No. MCEER-99-0002.
23. Trifunac MD, Brady AG. A study on the duration of strong earthquake ground motion. *Bulletin of the Seismological Society of America* 1975; **65**(3): 581-626.